Human Molecular Genetics, 2008, Vol. 17, No. 14 **2071–2083**
doi:10.1093/hmg/ddn106
Advance Access published on April 1, 2008

Striatal and nigral pathology in a lentiviral rat model of Machado-Joseph disease

Sandro Alves[1,2,7], Etienne Régulier[4,†], Isabel Nascimento-Ferreira[1,2], Raymonde Hassig[7,8], Noelle Dufour[7,8], Arnulf Koeppen[5], Ana Luísa Carvalho[1,3], Sérgio Simões[1,2], Maria C. Pedroso de Lima[1,3], Emmanuel Brouillet[7,8], Veronica Colomer Gould[6], Nicole Déglon[7,8] and Luís Pereira de Almeida[1,2,*]

[1]Center for Neurosciences and Cell Biology, [2]Faculty of Pharmacy and [3]Faculty of Sciences, University of Coimbra, Coimbra, Portugal, [4]Ecole Polytechnique Fédérale de Lausanne (EPFL), Brain Mind Institute, Lausanne, Switzerland, [5]VA Medical Center and Albany Medical College, Albany, NY, USA, [6]Department of Psychiatry, Johns Hopkins University School of Medicine, Baltimore, MA, USA, [7]CEA, Institute of Biomedical Imaging (I2BM) and Molecular Imaging Research Center (MIRCen), Fontenay-aux-Roses, France and [8]CNRS, URA2210, Orsay, France

Received February 5, 2008; Revised and Accepted March 29, 2008

Machado-Joseph disease (MJD) is a fatal, dominant neurodegenerative disorder. MJD results from polyglutamine repeat expansion in the MJD-1 gene, conferring a toxic gain of function to the ataxin-3 protein. In this study, we aimed at overexpressing ataxin-3 in the rat brain using lentiviral vectors (LV), to generate an *in vivo* MJD genetic model and, to study the disorder in defined brain regions: substantia nigra, an area affected in MJD, cortex and striatum, regions not previously reported to be affected in MJD. LV encoding mutant or wild-type human ataxin-3 was injected in the brain of adult rats and the animals were tested for behavioral deficits and neuropathological abnormalities. Striatal pathology was confirmed in transgenic mice and human tissue. In substantia nigra, unilateral overexpression of mutant ataxin-3 led to: apomorphine-induced turning behavior; formation of ubiquitinated ataxin-3 aggregates; α-synuclein immunoreactivity; and loss of dopaminergic markers (TH and VMAT2). No neuropathological changes were observed upon wild-type ataxin-3 overexpression. Mutant ataxin-3 expression in striatum and cortex, resulted in accumulation of misfolded ataxin-3, and within striatum, loss of neuronal markers. Striatal pathology was confirmed by observation in MJD transgenic mice of ataxin-3 aggregates and substantial reduction of DARPP-32 immunoreactivity and, in human striata, by ataxin-3 inclusions, immunoreactive for ubiquitin and α-synuclein. This study demonstrates the use of LV encoding mutant ataxin-3 to produce a model of MJD and brings evidence of striatal pathology, suggesting that this region may contribute to dystonia and chorea observed in some MJD patients and may represent a target for therapies.

INTRODUCTION

Machado-Joseph disease (MJD) or spinocerebellar ataxia type 3 (SCA3) is one of nine dominant neurodegenerative diseases resulting from polyglutamine repeat expansions. It was originally described in people of Portuguese descent, particularly from the Azores islands, where MJD is most prevalent (1:140 in the small island of Flores). It was subsequently identified in several other countries and is now considered to be the most common dominantly inherited hereditary ataxia (1).

MJD is caused by an unstable expansion of a CAG tract in the coding region of the gene, *MJD1* on chromosome 14q32.1 (2). *MJD1* encodes ataxin-3, a polyubiquitin-binding protein

*To whom correspondence should be addressed at: Center for Neurosciences and Cell Biology and Faculty of Pharmacy, University of Coimbra, R. Norte, 3000-295 Coimbra, Portugal. Tel: +351 966337482; Fax: +351 239827126; Email: luispa@ci.uc.pt or lpereiradealmeida@gmail.com
†Present address: Novartis, Target and Lead Discovery Unit, Basel, Switzerland.

whose physiological function has been linked to ubiquitin-mediated proteolysis (3–7). The mutation results in a long polyglutamine chain at the C-terminus of ataxin-3 (8); there are between 10 and 51 glutamine residues in the normal population and between 55 and 87 in MJD patients (9–11). There is a negative correlation between the age of onset and the number of CAG repeats, as is the case for other polyglutamine disorders (12).

The clinical hallmark of MJD is progressive ataxia, a dysfunction of motor coordination that can affect gaze, speech, gait and balance (13). Levodopa-responsive parkinsonism symptoms, among other clinical features, were also reported (14). In MJD patients, ataxin-3 is present in Marinesco bodies which are found in substantia nigra (15–17). The neuropathology of the disease involves multiple systems such as non-cortical cerebellar systems (particularly the dentate nucleus and pontine neurons), cranial nerve motor nuclei and substantia nigra (1,8). Recent studies suggest that other brain areas might be also affected in MJD. Positron emission tomography revealed low levels of fluorodopa uptake, dopamine transporter binding and regional cerebral glucose metabolism in the putamen of MJD patients (18–20). Some patients exhibit dystonia and more rarely chorea and these symptoms are not completely explained by cerebellar neuropathology, and could have contribution of striatal pathology (21). Dementia and delirium have also been reported suggesting that neuropathological changes might occur in the cortex (22).

Investigations of the neuropathology of the disease and evaluation of therapeutic approaches require animal models that closely mimic the human pathology. The development and study of various transgenic mouse models (23–26) have significantly contributed to our understanding of MJD. The localized overexpression of mutant protein using viral vectors has been a successful alternative for modeling pathologies of the central nervous system (CNS) (27–30). This strategy generates robust *in vivo* genetic models leading to neuronal degeneration in defined regions of the brain. Therefore, the aim of this work was to develop a lentiviral-based genetic model of MJD in the rat and to evaluate the pathology in different brain areas. In particular, we examined the substantia nigra, where overt neuropathological changes have been described in patients, and the striatum and cortex, which have been indirectly implicated in the pathology of the disease.

RESULTS

Strategy used to generate an *in vivo* model of Machado-Joseph disease in adult rats

The cDNA encoding human ataxin-3 with either 27 (normal; atx3-27Q) or 72 glutamines (mutant; atx3-72Q) and containing a Myc Tag at the 5′ end was inserted into the SIN-W-PGK lentiviral backbone (Fig. 1A) such that the transgene is under control of the phosphoglycerate kinase 1 (PGK) promoter, a housekeeping promoter which allows stable long-term expression (31). We validated these lentiviral vectors (LV) in 293T cells (Fig. 1B–D). Five days post-infection, both wild-type and mutant proteins were detected using immunocytochemistry with a myc antibody (Fig. 1C–D); no immunoreactivity (IR) was detected in non-infected cells (Fig. 1B). These results were confirmed by western blot with antibodies recognizing ataxin-3 (1H9), the expanded polyglutamine repeats (1C2) and the Myc epitope. In all cases, wild-type and mutant ataxin-3 proteins were detected at the predicted molecular weights and in similar amounts (Fig. 1E–G). The 1H9 antibody, which also recognizes the endogenous human ataxin-3 in 293T cells (Fig. 1E) revealed substantial overexpression of the transgenic forms (27Q and 72Q) of ataxin-3. Densitometric analysis showed that the amounts of transgenic (27Q and 72Q) ataxin-3 were six times higher than those of endogenous ataxin-3 (1H9 antibody). As expected, a more robust IR signal was detected with the 1C2 antibody for mutant ataxin-3-expressing cells than for cells expressing wild-type ataxin-3 (Fig. 1F).

In vivo, upon injection of the vectors in the rat brain human wild-type and mutant ataxin-3 were also detected by western blot on tissue punches (Supplementary Material, Fig. S1). The level of transgenic wild-type ataxin-3 was four times higher than the endogenous rat ataxin-3 (Supplementary Material, Fig. S1A) indicating that LV allows robust overexpression of ataxin-3 *in vivo*.

Induction of a Machado-Joseph disease neuropathology in different regions of the rat brain

We chose the substantia nigra as the reference area for the establishment of the SCA3 model because this region is affected in MJD patients, causing Parkinson's disease-like symptoms (Fig. 2A) (14). In addition, we injected vectors into the striatum and cortex, regions which might also be involved in the disease (Fig. 2A).

Accumulation of ubiquitinated and α-synuclein-positive aggregates following mutant ataxin-3 expression in the substantia nigra

Wild-type and mutant ataxin-3 were detected in the substantia nigra 2 months after lentiviral injection, using the 1H9 antibody (Fig. 2B–D). Intense staining revealed production of a substantial amount of both ataxin-3 species. The wild-type ataxin-3 signal was diffuse, covering all subcellular structures (Fig. 2B and C), whereas mutant ataxin-3 (72Q) detection resulted in punctate and mainly nuclear staining (Fig. 2D and E). This pattern suggests formation of nuclear ataxin-3 inclusions, characteristic of the disease (32).

We then used confocal microscopy to investigate whether the mutant ataxin-3 inclusions co-localize with ubiquitin and α-synuclein, two proteins involved in Parkinson's disease. As expected, no ubiquitin-IR or α-synuclein-IR was detected in the regions injected with vectors encoding wild-type ataxin-3 (27Q) (Fig. 2F and I). In contrast, within the regions expressing mutant ataxin-3, 1H9-positive aggregates were immunoreactive for ubiquitin (Fig. 2G and H). Moreover, a considerable number of ataxin-3 aggregates ($42 \pm 8\%$) were also immunoreactive for α-synuclein (Fig. 2J).

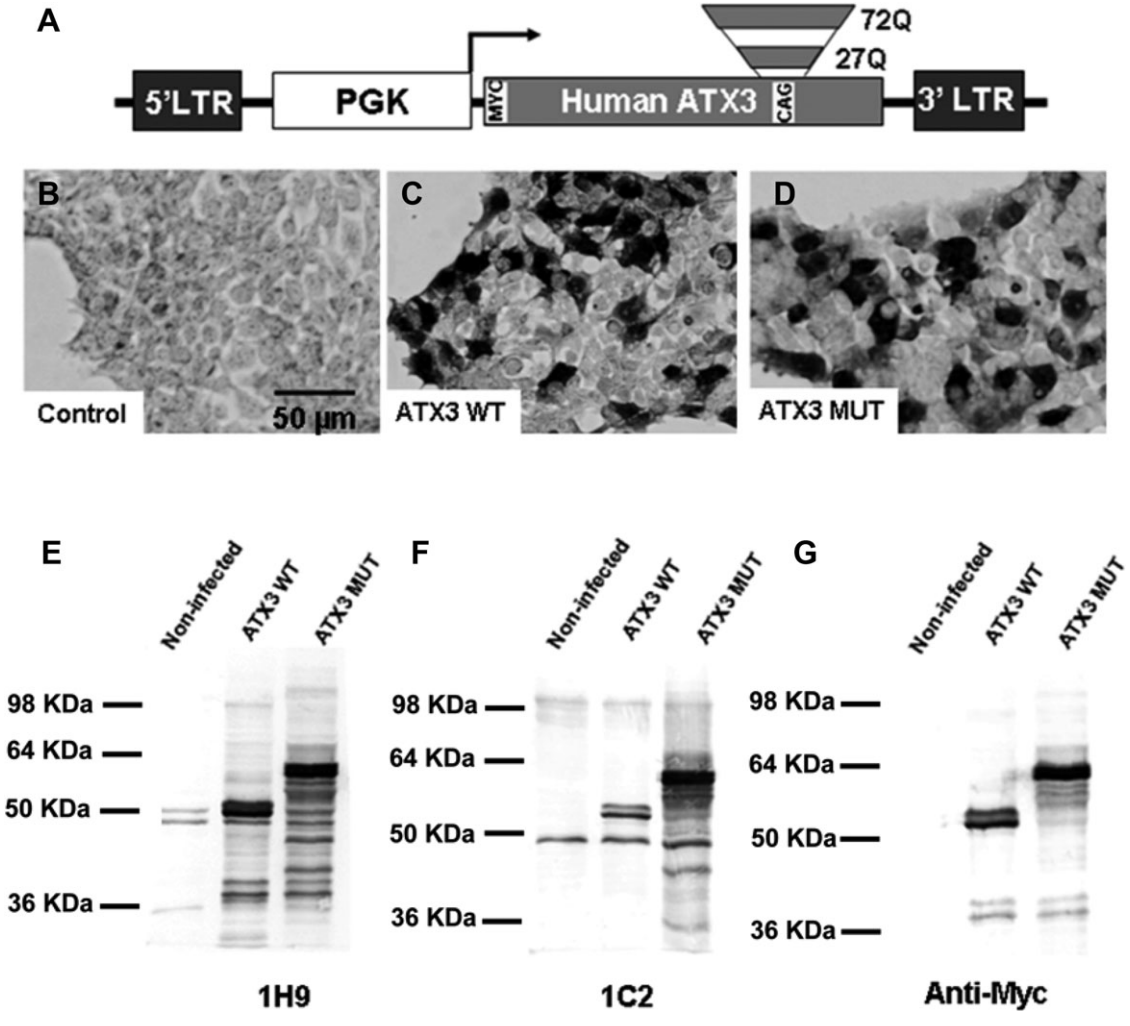

Figure 1. (**A**) Schematic representation of the lentiviral constructs used in the development of the animal model of Machado-Joseph disease. cDNAs encoding human wild-type (27 CAG repeats) or mutant ataxin-3 (72 CAG repeats) were cloned in the SIN-W transfer vector. (**B**–**D**) Infection of 293T cells with wild-type human ataxin-3 (ATX3 WT /27Q) (C) or mutant human ataxin-3 (ATX3 MUT/72Q) (D) encoding vectors containing a human Myc epitope tag at the 5′ end [anti-Myc tag (OP10) antibody (1:200)]. (**E**–**G**) The western blot analysis of 293T cells infected with lentiviral vectors encoding ATX3 WT or ATX3 MUT at 1 week post-infection. The membranes were probed with the antibodies anti-ataxin-3 (1H9) (E), 1C2 (F) and anti-Myc tag (G).

Expression of mutant ataxin-3 causes depletion of neurons immunoreactive for tyrosine hydroxylase and vesicular monoamine transporter 2

We tested whether overexpression of mutant ataxin-3 was associated with neuronal dysfunction by immunohistochemical analysis with two markers of dopaminergic neurons, the tyrosine hydroxylase (TH) and the vesicular monoamine transporter 2 (VMAT2). Loss of TH- and VMAT2-IR was observed in ataxin-3-72Q-injected animals (Fig. 3A and D) and high magnification shows a high depletion of TH-positive cells around the injection site (Fig. 3A). Double staining for TH and ataxin-3 further confirmed the depletion of TH in expressing neurons (Supplementary Material, Fig. S2B). In contrast, TH-IR co-localized with 1H9-IR in wild-type ataxin-3 expressing neurons (Supplementary Material, Fig. S2A). Quantitative analysis revealed a reduction in the number of TH-IR neurons to 61.4 $\pm$ 8.5% when compared with the non-injected hemispheres, and no reduction of TH-IR in wild-type ataxin-3-injected hemispheres (Fig. 3B). A reduction of TH immunoreactivity was also observed in the striatum of animals injected with LV encoding mutant ataxin-3 suggesting dysfunction of the TH nigro-striatal projecting fibers (Fig. 3C). Neuronal dysfunction was further demonstrated in sections stained with a VMAT2 antibody. A significant reduction in the number of neurons immunoreactive for VMAT2 was observed in animals injected with the LV expressing mutant ataxin-3, but not in those injected with the wild-type protein (Fig. 3D and Supplementary Material, Fig. S2C and D).

Behavioral deficit induced by mutant ataxin-3 expression in the substantia nigra

To evaluate whether the neuropathological changes induced by mutant ataxin-3 overexpression induced a Parkinson-like behavioral dysfunction, a group of animals submitted to unilateral injection of the mutant ataxin-3 encoding vector into

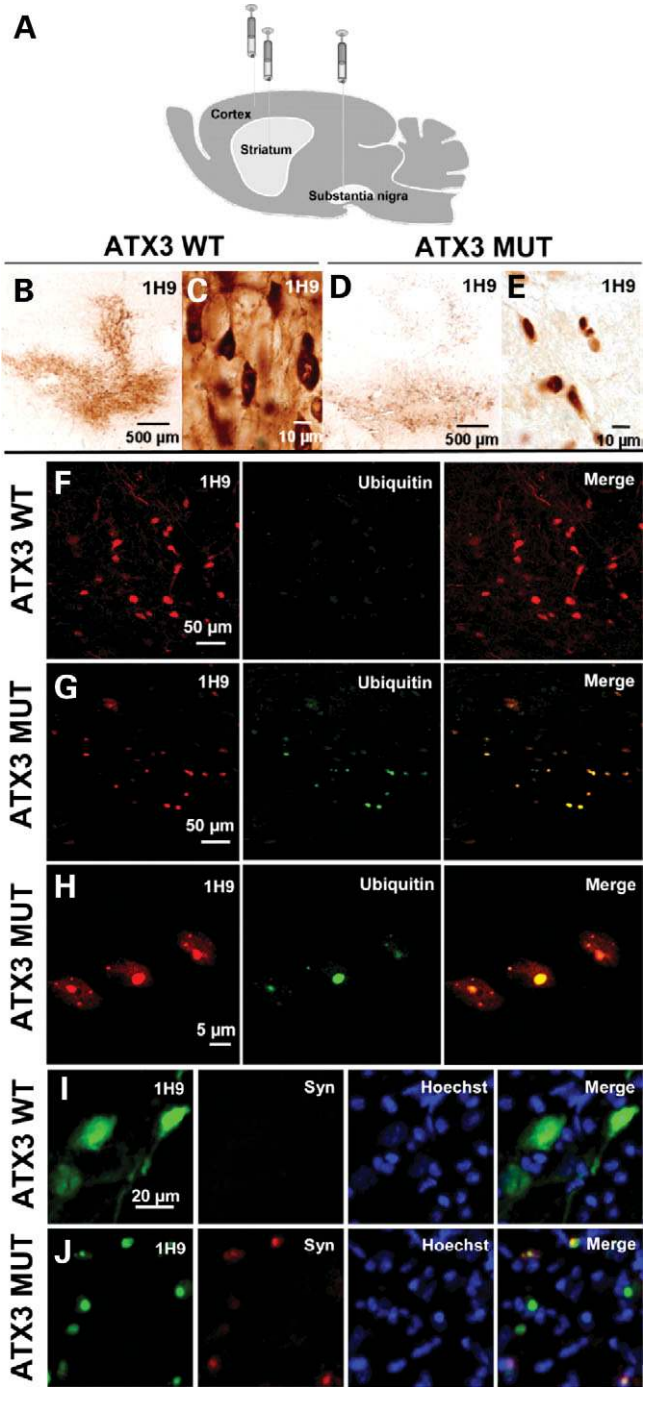

Figure 2. (**A**) Rat brain regions targeted with the human ataxin-3-encoding lentiviral vectors. Human ataxin-3 overexpression in the adult rat brain at 2 months; (**B**) intranigral injection of wild-type or (**D**) mutant ataxin-3 in adult rats; (**C**) anti-ataxin-3 staining (1H9) showing the expression of the wild-type protein in the cytoplasm and (**E**) the translocation of the mutant ataxin-3 to the nucleus. (**G** and **H** at high magnification) Overexpression of mutant ataxin-3 in substantia nigra neurons promotes formation of ubiquitinated ataxin-3 aggregates. (**F**) In contrast, no evidences of aggregation were observed when wild-type ataxin-3 was overexpressed. (**I** and **J**) Counterstaining with the Hoechst dye demonstrates that overexpression of mutant ataxin-3 in substantia nigra induces the formation of α-synuclein-positive aggregates in the nucleus (J), whereas overexpression of wild-type ataxin-3 does not promote the formation of α-synuclein positive nuclear aggregates (I).

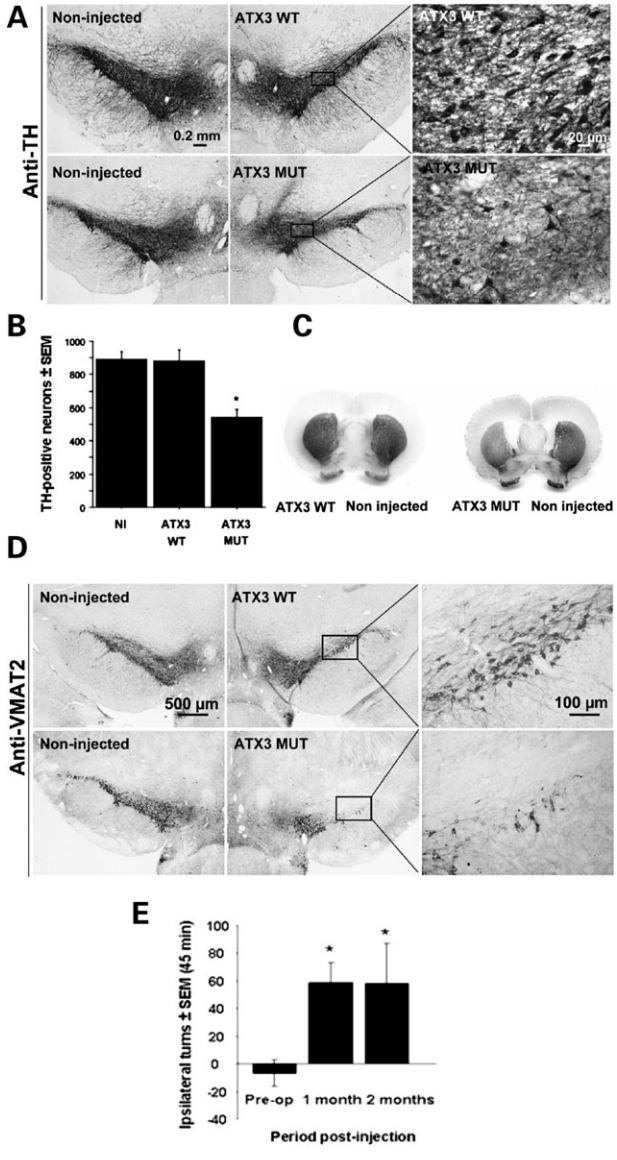

Figure 3. Neuropathology. (**A**) Depletion of tyrosine hydroxylase (TH)-positive neurons in the substantia nigra caused by overexpression of mutant ataxin-3, suggesting neuronal dysfunction; whereas overexpression of wild-type ataxin-3 has no deleterious effect at 2 months (i.e. no significant difference between injected and non-injected (NI) hemispheres). (**B**) Quantitative analysis of the number of TH-positive neurons in adult rat brains injected in the susbstantia nigra with human ataxin-3 ($^{*}P < 0{,}001$ when compared with all groups). (**C**) Striatal TH down-regulation in animals injected in the substantia nigra with mutant ataxin-3, suggesting degeneration of the nigro-striatal pathway. The intranigral injection of wild-type ataxin-3 does not induce TH downregulation in the striatum. (**D**) Reduction of the number of vesicular monoamine transporter type 2 (VMAT2)-immunoreactive neurons in the substantia nigra caused by overexpression of mutant ataxin-3, suggesting neuronal dysfunction; whereas overexpression of wild-type ataxin-3 has no deleterious effect at 2 months (no significant difference between injected and non-injected (NI) hemispheres). (**E**) Behavioral analysis: apomorphine-induced turning in adult rats unilaterally lesioned with mutant ataxin-3 in the substantia nigra. Results are expressed as the net difference between the total number of turns after and before lesion. Ipsilateral turns were counted as positive turns, whereas contralateral turns were counted as negative turns. Rotational behavior statistical significance was evaluated using the Friedman test, a non-parametric test for paired samples ($P = 0.018$).

the substantia nigra were tested for rotational asymmetry. Animals injected with the mutant ataxin-3-virus displayed more ipsilateral turning in response to the dopamine agonist apomorphine than before injection (Fig. 3E). This motor deficit was still detected 2 months post-injection demonstrating stability of the neuronal dysfunction.

Injection of mutant ataxin-3 in the cortex

Neuropathological examination of MJD brains indicates that the substantia nigra, pontine nuclei, cerebellar dentate nucleus, cranial nerve nuclei, spinal anterior horns and Clarke's columns are the major regions of degeneration (1). However, there is growing clinical data and neuroradiological evidence of striatal and cerebral cortex dysfunction in some MJD patients (18,20,33,34). The western blot analysis indicated that the ataxin-3 is expressed not only in the substantia nigra, but also in the cortex and striatum (Fig. 4A). LV encoding wild-type and mutant ataxin-3 were injected in the cortex to assess the potential involvement of this structure in MJD pathology. After 3 months, both wild-type and mutant ataxin-3 were detected over a large region. A diffuse pattern of wild-type ataxin-3 immunoreactivity was observed (Fig. 4B and D), whereas numerous ubiquitin-positive nuclear inclusions were detected with the mutant ataxin-3 (Fig. 4C, E and G). No significant modification of the neuronal marker NeuN was detected by immunostaining (Fig. 4I), except in a region immediately surrounding the needle tract. These data suggest that the presence of ataxin-3 nuclear inclusions in the cortex is not associated with major neuropathological changes, even 3 months post-injection of the vectors.

Striatal neuropathology due to mutant ataxin-3 overexpression

To investigate the involvement of the striatum in MJD pathology, we injected LV encoding wild-type and mutant ataxin-3 into this brain region. At 2 weeks (Supplementary Material, Fig. S3) and 2 months post-injection (Fig. 5, 6 and Supplementary Material, Fig. S4), aggregation of mutant ataxin-3, accompanied by ubiquitination (Fig. 5B, D, F and Supplementary Material, Fig. S3A and E), was detected. Additionally, at 2 months there was condensation of the cell nucleus (Fig. 5H), loss of NeuN-IR (Fig. 5J) and DARPP-32-IR (Supplementary Material, Fig. S4B), condensation of the internal capsule of the striatum (Fig. 5L) and fluorojade B-positive cells (Fig. 5N) within the region transduced with mutant ataxin-3, whereas the hemisphere overexpressing wild-type ataxin-3 was unaffected (Fig. 5G, I, K, M and Supplementary Material, Fig. S4A and C). Importantly, the severity of the pathology was dose- and time-dependent (Supplementary Material, Figs S5 and S3); indeed, animals injected with 500 ng p24 and 1000 ng p24 of the vectors encoding mutant ataxin-3 had DARPP-32-depleted volumes of 1.12 ± 0.06 and 1.51 ± 0.08 mm^3, respectively, 2 months post-injection (Supplementary Material, Fig. S5E–I), and no NeuN or DARPP-32 loss of immunoreactivity at 2 weeks (Supplementary Material, Fig. S3C and D).

Regarding the subcellular localization of ataxin-3, wild-type protein displayed 1H9-IR throughout cell bodies (Fig. 6A) without ubiquitin-IR (Fig. 6A), as observed using confocal microscopy. Wild-type ataxin-3 immunoreactivity co-localized with DARPP-32 and NeuN stainings (Supplementary Material, Fig. S4A and C). High magnification revealed that wild-type ataxin-3 accumulated close to the nuclear envelope (Fig. 6C). In contrast, mutant ataxin-3 inclusions (Fig. 6D) are localized in dense intranuclear aggregates which were

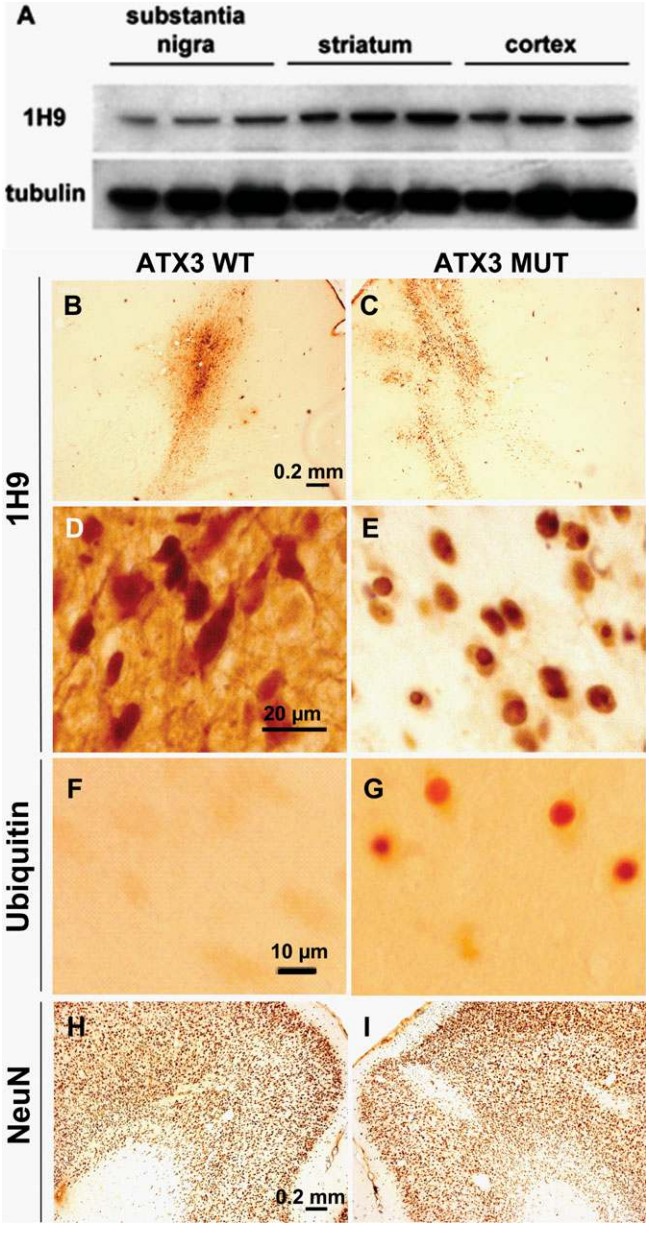

Figure 4. (**A**) Western blot showing the endogenous expression of ataxin-3 in the substantia nigra, striatum and cortex of the adult rat brain. For each brain region, 10, 20 or 30 µg of protein were loaded, respectively. (**B** and **C**) Anti-ataxin-3 staining (1H9) showing the efficient transduction of adult rat cortical neurons with human ataxin-3 expressing lentiviral vectors. (**D**) Expression of wild-type protein occurs both in the cytoplasm and nucleus, whereas mutant ataxin-3 is translocated to the nucleus (**E**) promoting the formation of ubiquitin-positive nuclear inclusions, at 3 months (**G**). No overt change in NeuN staining was observed after wild-type (**H**) or mutant (**I**) ataxin-3 expression in the rat cortex, excepting the needle tract area.

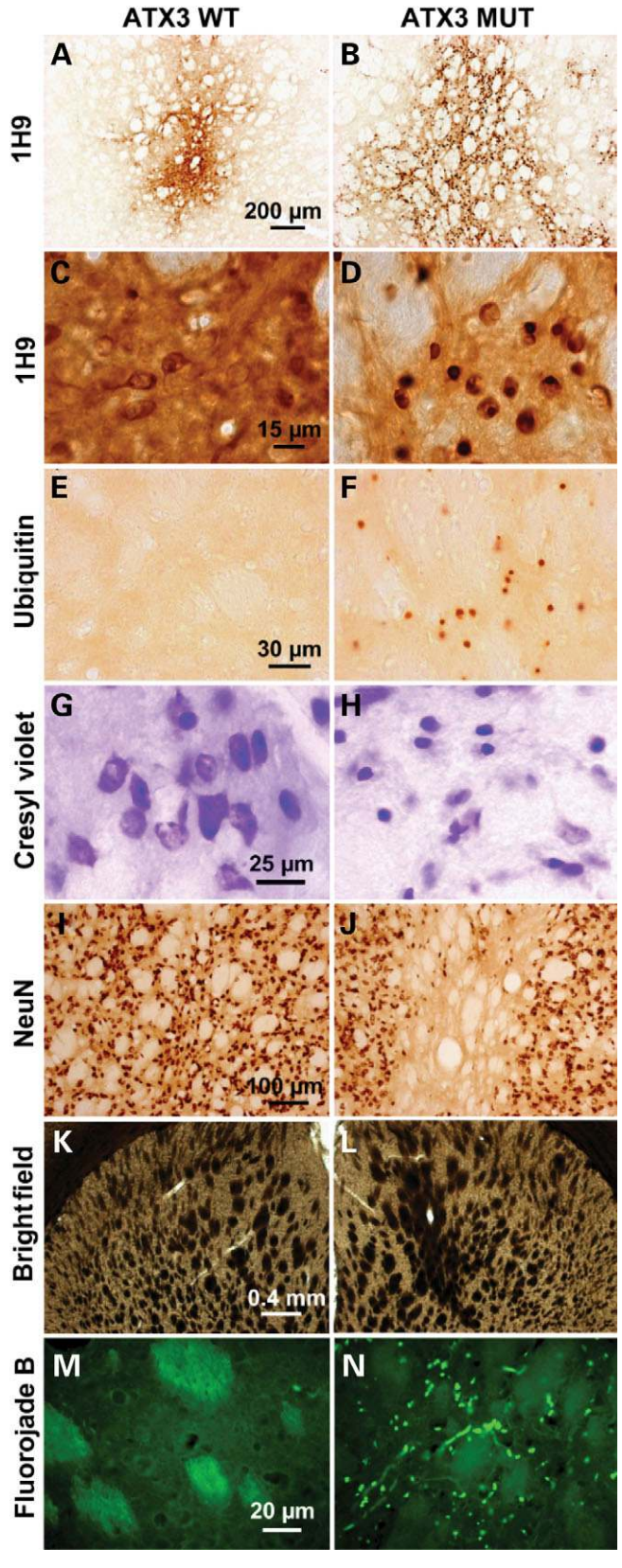

Figure 5. (**A** and **B**) Striatal injection of wild-type and mutant human ataxin-3 in the adult rat brain. Anti-ataxin-3 staining (1H9) showing expression of the wild-type protein in the cytoplasm (**C**) and translocation of the mutant ataxin-3 to the nucleus (**D**) inducing the formation of ubiquitin-positive aggregates at 2 months (**F**). (**H**) Pycnotic nuclei are visible on cresyl violet stained sections suggesting possible cell injury and striatal degeneration after injection of vectors encoding mutant ataxin-3 in adult rats, at 2 months. (**J**) A considerable loss of NeuN-immunoreactive neurons was observed in the region expressing mutant ataxin-3, whereas wild-type ataxin-3 (**I**) has no toxic effect. (**L**) Coalescence of the internal capsule of the striatum was observed after mutant ataxin-3 expression at 2 months on a bright-field photomicrograph, suggesting degeneration. (**K**) In contrast, no signs of coalescence were observed when wild-type ataxin-3 was expressed. (**N**) Striatal degeneration in mutant ataxin-3-injected rats observed at 2 months post-injection on Fluorojade B stained sections in contrast with wild-type ataxin-3-injected rats (**M**).

ubiquitin-IR (Fig. 6B). In addition, at the center of the injected region, where transgene expression levels are highest, a loss of ataxin-3-IR (1H9), NeuN-IR or DARPP-32-IR immunoreactivity was observed, presumably due to cell degeneration (Supplementary Material, Fig. S4B and D). Western blot from striatal tissue punches revealed enrichment of wild-type ataxin-3 in the supernatant fraction (Supplementary Material, Fig. S1A and B), while mutant ataxin-3 was mainly detected in the insoluble fraction. In this fraction, high molecular weight species of mutant ataxin-3 immunoreactive for ubiquitin were visible (Supplementary Material, Fig. S1C and D). Very faint bands possibly corresponding to cleavage fragments were also detected. Additional studies are, however, warranted to further investigate the processing and appearance of cleavage fragments.

These results, suggest that the striatum is directly involved in Machado-Joseph pathology, improve our understanding of the pathogenesis of the disorder and may help in the development of therapy.

Striatal pathology in MJD transgenic mice and patient tissue

To further confirm the involvement of the striatum in the pathology, MJD transgenic mice (25) and post-mortem striatal sections of MJD patient's brains were analyzed by immunohistochemistry. Ubiquitinated ataxin-3 aggregates were detected throughout striata of Q71C homozygous transgenic mice (Fig. 7B, C, E, F and Supplementary Material, Fig. S6B), whereas no aggregates were detected in wild-type mice (Fig. 7A, D and Supplementary Material, Fig. S6A). DARPP-32 staining revealed a substantial downregulation of DARPP-32 (Fig. 7H and Supplementary Material, Figs S6D and S7), suggesting a striatal dysfunction at 10–13 weeks. Similar analysis was performed with striatal tissue from three human patients (61 ± 6 years, 71 ± 3 CAG). Despite technical difficulties associated with the long fixation times – preventing DARPP-32 immunostaining – ubiquitinated ataxin-3 inclusions were detected in the striata of the three MJD patients (Fig. 7L, M, O and Supplementary Material, Fig. S8). Moreover, immunoreactivity for α-synuclein co-localizing with ataxin-3-IR was identified in intranuclear and perinuclear inclusions found in human tissue (Fig. 7Q, R and Supplementary Material, Fig. S8B, C, D and E). Conversely, inclusions were absent from control tissue (Fig. 7K, N and P), thus demonstrating neuropathology in this region in patients.

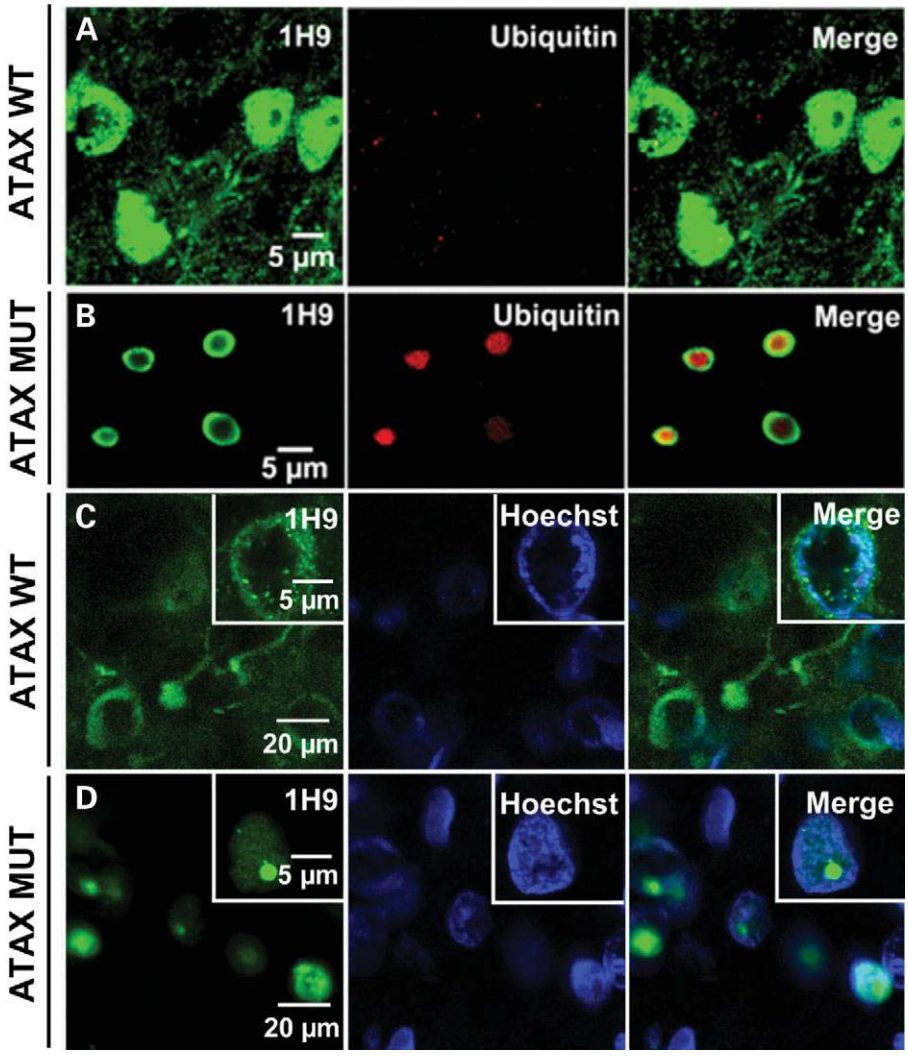

Figure 6. Overexpression of wild-type or mutant human ataxin-3 in the adult rat striatum, subcellular distribution and interaction with different proteins. (**B**) Expression of mutant human ataxin-3 induces the formation of aggregates which are ubiquitinated particularly within the central core of the intranuclear inclusions; (**A**) whereas expression of wild-type ataxin-3 is cytoplasmatic and does not promote the formation of intranuclear ubiquitin-positive inclusions; (**C**) cell nuclei counterstained with Hoechst dye demonstrate that expression of wild-type ataxin-3 is predominantly perinuclear and cytoplasmatic whereas mutant ataxin-3 is nuclear (**D**).

DISCUSSION

In this study, we used LV to develop an *in vivo* model of MJD. We showed that LV allow robust expression of human ataxin-3 in rat brain. Lentiviral-mediated expression of mutant but not wild-type ataxin-3 induced behavioral and neuropathological abnormalities associated with MJD, supporting our strategy to develop an animal model of MJD.

In the first part of the study, we investigated pathological changes at the substantia nigra, an area affected in MJD. There are various observations implicating this area in MJD: (i) levodopa-responsive parkinsonism has been reported in patients (14); (ii) neuropathology has been described in substantia nigra of affected individuals (1,8); (iii) transgenic mice expressing mutant ataxin-3 (Q71) develop a pathological phenotype with decreased TH-IR neurons in the substantia nigra (25); and (iv) even non-expanded ataxin-3 is found in intranuclear aggregates within Marinesco bodies in human and non-human primate substantia nigra (15–17).

Transduction of substantia nigra with LV encoding either wild-type or mutant ataxin-3 resulted in robust transgene expression. Wild-type ataxin-3 was evenly distributed throughout the cell, particularly around the nuclear envelope, whereas mutant ataxin-3 accumulated into dense neuronal intranuclear aggregates and was depleted from the cytoplasm. Even though a nuclear localization signal (NLS) has been identified upstream from the polyglutamine repeat region of ataxin-3 (35), the non-expanded protein is present both in the nucleus and in the cytoplasm (36); indeed, ataxin-3 possesses nucleocytoplasmic shuttling activity (37). Moreover, recent data showing that nuclear localization of ataxin-3 is required for the manifestation of symptoms in MJD have emerged (26). It has been suggested that the nuclear environment favors a conformation of wild-type ataxin-3 that is more likely to aggregate (38,39). Although the role of aggregates in MJD remains controversial, they are

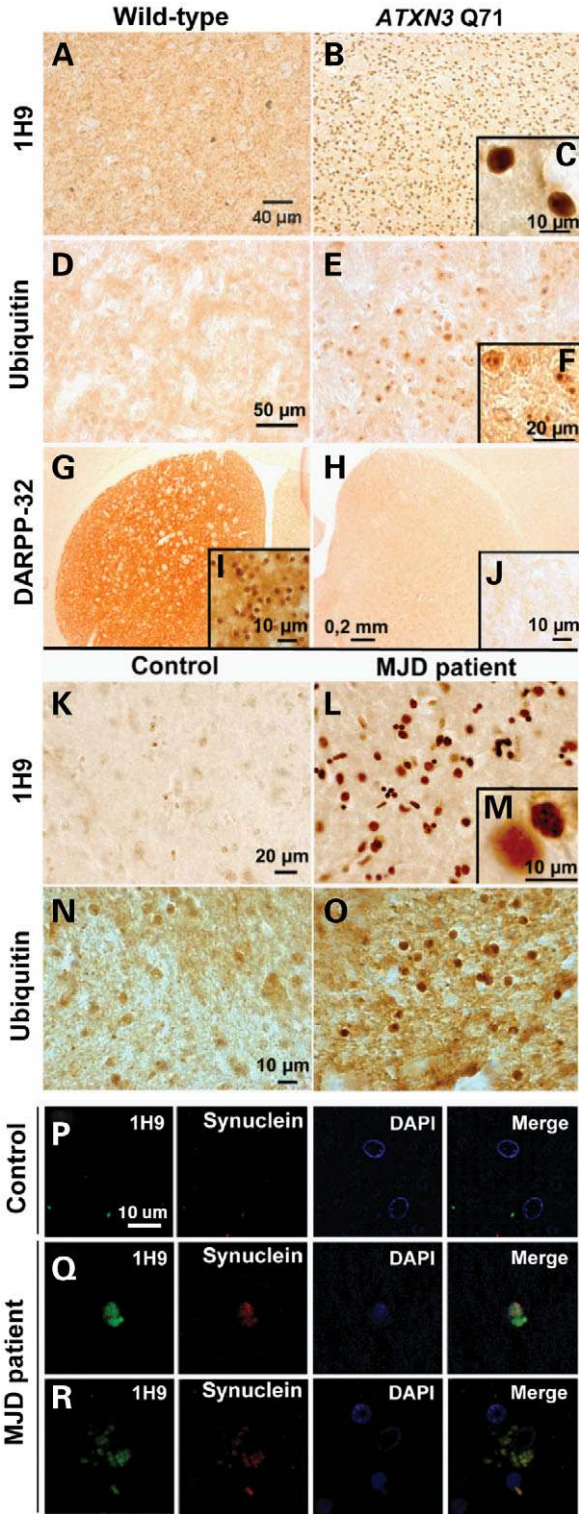

Figure 7. Ataxin-3 (1H9) immunohistochemical staining in wild-type mice (**A**) and *ATXN3* Q71C homozygous transgenic mice (**B**). (**B**) Ataxin-3 immunoreactive aggregates are observed in *ATXN3* Q71C homozygotes. (**C**) At higher magnification, nuclear inclusions adjacent to the nucleolus are observed. (**E** and **F** with a high magnification) Ubiquitin-positive inclusions are present in *ATXN3* Q71C homozygotes and are not observed in wild-type animals (**D**). (**H** and **J** with high magnification) *ATXN3* Q71C homozygotes express lower levels of DARPP-32 than wild-type mice suggesting possible neuronal dysfunction (**G** and **I** with high magnification). (**N**) The striata of MJD patients contain ubiquitin-(**O**) and ataxin-3-(**L**) positive aggregates with distinct nuclear inclusions (**M**) when compared with the control brains (**N** and **K**, respectively). (**P**–**R**) Ataxin-3 and α-synuclein immunoreactivity in brain sections from a MJD patient. Shown are representative confocal laser micrographs from the striata of a MJD patient showing co-localization of α-synuclein and ataxin-3. (**Q**) and (**R**) show intranuclear (**Q**) and intracytoplasmic (**R**) co-localization of ataxin-3 and α-synuclein.

typical of polyglutamine disorders and have been used as indicators of disease progression.

In MJD patients expanded ataxin-3 accumulates in ubiquitinated neuronal intranuclear inclusions (NII) within affected brain regions (40). Polyglutamine expansion causes ataxin-3 monomeric peptides, which exist predominantly in a random coil conformation, to aggregate into ß-rich amyloid-like fibrillar structures (41). Expansion of the glutamine repeat in ataxin-3 destabilizes the native protein structure leading to the formation of fibrillar aggregates with increased ß-structure and the ability to bind the amyloid dye, Congo red (42). This implies that MJD shares pathogenic mechanisms with other amyloid-associated diseases such as Alzheimer's and prion's diseases. The identity of the pathogenic species remains unknown – whether the protein alone, the putative intermediates of the fibrillization pathway, or the soluble mature fibrils (43,44). Nevertheless, similarities with other misfolding amiloidopathies suggest that small initial aggregates, such as the recently identified protofibrillar intermediates (43–45), may be more toxic than large aggregates (46). While, further studies are necessary to confirm and identify the presence of these intermediates, our results in striatal homogenates clearly show an accumulation of mutant ataxin-3 as insoluble and high molecular weight species.

Another feature of mutant ataxin-3 aggregates was the presence of ubiquitin, a molecule which is closely associated with the proposed function and structure of ataxin-3. Depending on the isoform, ataxin-3 has two to three ubiquitin-interacting motifs (UIMs). It has been suggested that ataxin-3 removes ubiquitin from substrates to allow proteosomal degradation (47). Therefore, these motifs would bind ubiquitin from poly-ubiquitinated substrates, allowing cleavage by the ataxin-3 N-terminal Josephin domain (48). The presence of ubiquitin in ataxin-3 aggregates may also be a consequence of ataxin-3 itself being a substrate for ubiquitination, and thus being degraded by the ubiquitin–proteasome pathway (49,50). We found that α-synuclein, a presynaptic protein widely expressed in the brain and associated with Parkinsonism, co-localizes with ataxin-3 inclusions in rat substantia nigra and human striatum. α-Synuclein may be recruited into ataxin-3 aggregates due to the propensity of this protein and its ubiquitinated form to interact with the UIMs present in ataxin-3. Non-expanded ataxin-3 has been reported to be present in intranuclear aggregates within Marinesco bodies found in human and non-human primate substantia nigra (15–17); thus ataxin-3 may promote α-synuclein proteolysis. Proteolytic activity of wild-type ataxin-3 suppresses neurodegeneration induced by mutant ataxin-3 in a *Drosophila* MJD model (51). Further studies should be conducted to evaluate the relationship between these two proteins.

In addition to the accumulation of NII, we observed a substantial loss of TH and VMAT2 staining within the transduced

area in the substantia nigra. No co-localization of TH or VMAT with mutant ataxin-3 was observed. These data are in line with the reduction of TH-positive cells reported in transgenic models of MJD (24,25). Moreover, depletion of the number of neurons immunoreactive for TH in the substantia nigra was accompanied by a similar, although less pronounced reduction of TH immunoreactivity in the striatum, indicating a loss of function of dopaminergic neuron terminals within the striatum. These animals displayed rotational behavior under apomorphine, further corroborating these neuropathological observations.

MJD is characterized by degeneration of brain regions in addition to the substantia nigra (1,8). Recently, imaging techniques of MJD patient brains implicated two other areas, the cerebral cortex and the striatum. In this study, we evaluated the neuropathological effects of mutant ataxin-3 local overexpression in these regions. In the cortex, the overexpression of mutant ataxin-3 was associated with a minor loss of NeuN expression, in contrast to the severe pathology observed at 2 months in the substantia nigra. The cortical accumulation of ubiquitinated ataxin-3 aggregates might nevertheless lead to neuronal dysfunction and may explain the decrease in cerebral glucose metabolism identified by positron emission tomography in the cerebral cortex (18,19).

The third region that we targeted with LV was the striatum. We found a dose-dependent loss of neuronal markers, an accumulation of NII and high molecular weight species, and finally cell death. Such striatal pathology was unexpected, because there were no clear evidences of neuropathology for this region in MJD. Imaging studies in MJD patients provided indirect evidence that the striatum could be affected (18,19,52). Yen *et al.* (20) examined dopamine transporter binding at nigrostriatal terminals of patients using single-photon emission computed tomography. Asymptomatic MJD gene carriers showed low levels of dopamine uptake in putamen, suggesting that impairment of pre-synaptic dopamine function occurs at an early stage. Data gathered in our rat model, in transgenic mice and in human tissue, demonstrate for the first time the involvement of this structure in MJD. The potential implication of the striatum in MJD provides an explanation for symptoms found in MJD patients (21) particularly the fairly common dystonia, and the more rare chorea. In animal models and in cerebral imaging and necropsies of patients, chorea and dystonia have been consistently associated with lesions in the striatum. Chorea seems to involve dysfunction of the indirect pathway from the caudate and putamen to the internal globus pallidus, whereas dystonia is generated by dysfunction of the direct pathway (53). Our results indicate that brain delivery of mutant ataxin-3 with LV provides a new genetic model of MJD which may help elucidate the molecular mechanism of mutant ataxin-3 toxicity and will facilitate the evaluation of new therapeutic strategies.

MATERIALS AND METHODS

Lentiviral vector production

cDNAs encoding the human wild-type ataxin-3 (Atx3-27Q) or mutant ataxin-3 (Atx3-72Q) (genbank: S75313), isoform mjd1a, kindly provided by Pittman and co-author (40), were cloned in the SIN-W-PGK transfer vector (27). Viral vectors were produced in 293T cells using a four-plasmid system described previously (54). The lentiviral particles were produced and resuspended in phosphate-buffered saline (PBS) with 1% bovine serum albumin (BSA) and samples were matched for particle concentration by measuring HIV-1 p24 antigen content (RETROtek, Gentaur, France). Viral stocks were stored at -80°C until use.

Western blot analysis

293T cells were infected with LV (300 ng of p24 antigen/well) and cultured with fresh D-MEM (Gibco, Paisley, Scotland, UK) containing 10% fetal bovine serum (FBS; Gibco, Paisley, Scotland, UK), 2 mM L-glutamine, 4500 mg/l glucose, 25 mM HEPES, 100 U/ml penicillin and 100 U/ml streptomycin (Gibco, Paisley, Scotland, UK). Cellular lysates were harvested 7 days post-infection in lysis buffer (150 mM NaCl, 50 mM Tris-base, pH 7,4, 5 mM EDTA, 0.5% Triton, 1% NP 40 and 0.5% protease inhibitor cocktail; Sigma). Protein concentration was determined with the Bradford protein assay (BioRad, Munich, Germany). Twenty microgram aliquots of the protein extracts were resolved on 12% SDS-polyacrylamide gels and transferred onto nitrocellulose membranes (Schleicher & Schuell Bioscience, Germany). Immunoblotting was performed using anti-ataxin-3 antibody (1H9; 1/1000; Chemicon, Temecula, CA, USA); anti-polyglutamine tract antibody (1C2; 1/1000; Chemicon, Temecula, CA, USA); anti-Myc tag antibody clone 4A6 (Upstate, Cell Signalling Solutions, NY, USA; 1/500), followed by incubation with an alkaline phosphatase-coupled goat anti-mouse antibody (1:5000; Sigma, St Louis, MO, USA). The presence of antigens was observed using a BCIP/NBT alkaline phosphatase substrate solution (SIGMA, St Louis, MO, USA).

In vitro immunocytochemistry

293T cells were infected with LV (150 ng of p24 antigen/well) and cultured with fresh D-MEM (Gibco, Paisley, Scotland, UK) containing 10% FBS (Gibco, Paisley, Scotland, UK), 2 mM L-glutamine, 4500 mg/l glucose, 25 mM HEPES, 100 U/ml penicillin and 100 U/ml streptomycin (Gibco, Paisley, Scotland, UK). Five days post-infection, the cell cultures were washed with PBS and fixed with paraformaldehyde (PAF) 4% in PBS. Immunostaining was performed using the primary monoclonal anti-Myc tag antibody clone 4A6 (Upstate, Cell Signalling Solutions, NY, USA) diluted in PBS/0.1% Triton X-100 containing 10% Normal Goat Serum (NGS; 1/500; Gibco, Paisley, Scotland, UK), followed by incubation with a biotinylated anti-mouse secondary antibody (1:200; Vector Laboratories). Bound antibodies were visualized using the Vectastain ABC kit, with 3,3′-diaminobenzidine tetrahydrochloride (DAB metal concentrate; Pierce) as substrate.

In vivo experiments

Adult male Wistar rats (Iffa Credo/Charles River, Les Oncins, France), weighing $\sim$200 g were used. The animals were housed in a temperature-controlled room and maintained on

a 12 h light/dark cycle. Food and water were available *ad libitum*. The experiments were carried out in accordance with the European Community Council directive (86/609/EEC) for the care and use of laboratory animals.

Endogenous rat ataxin-3 and human ataxin-3 detection by western blot

Brain punches of substantia nigra, cortex and striatum of adult rats were collected and processed to evaluate endogenous ataxin-3 levels. To analyse the *in vivo* expression of human ataxin-3, brain punch biopsies of 2.0 mm in diameter were obtained by dissection of striatal injected areas on dry ice after slicing the brain in a rat slicer matrix with 2.0 mm coronal slice intervals. Brain sections were snap-frozen on dry ice and stored at −80°C. Frozen tissue was prepared for immunoblot analysis by placing in the lysis buffer previously described followed by probe sonication. Samples were then frozen in liquid nitrogen three times and centrifuged for 30 min at 14 000 g to remove insoluble material, obtaining the supernatant fraction. Protein concentration was determined with the Bradford protein assay (BioRad, Munich, Germany). The pellet fraction was then resuspended in 2% SDS. The blotting procedure was similar to the one previously described. The antibodies used were the following: anti-ataxin-3 antibody (1H9; 1/1000; Chemicon, Temecula, CA, USA); anti-Myc tag antibody clone 4A6 (1/500; Upstate, Cell Signalling Solutions, NY, USA); anti-tubulin antibody (1:10000; Sigma, Saint Louis, MO, USA) and anti-ubiquitin antibody (1:1000; Dakocytomation, Zug, Switzerland). Blots were washed followed by incubation with the respective IgG HRP-coupled biotinylated goat secondary antibody (1:5000; Vector Laboratories, Burlingame, CA, USA) for 1 h at RT. The presence of antigens was observed using Enhanced Chemilunescence Reaction (ECL+, Amersham Pharmacia Biotech, Les Ulis, France).

In vivo injection of lentiviral vectors

Concentrated viral stocks were thawed on ice and resuspended by repeated pipetting. LV encoding human wild-type (Atx3-27Q) or mutant ataxin-3 (Atx3-72Q) were stereotaxically injected into the substantia nigra, cortex or striatum of anesthetized animals. Animals were anesthetized by administration of ketamine (75 mg/kg, i.p.) and xylazine (10 mg/kg, i.p.). Particle contents were determined by p24 antigen ELISA (RETROtek, Gentaur, France) and the appropriate amounts were injected into the different rat brain areas through a 34-gauge blunt-tip needle linked to a Hamilton syringe (Hamilton, Reno, NV, USA) by a polyethylene catheter.

Injection in the substantia nigra, cortex and striatum

LV expressing human wild-type (Atx3-27Q) ($n = 7$) or mutant ataxin-3 (Atx3-72Q) ($n = 6$) were unilaterally injected into the substantia nigra. The viral suspensions (125 000 ng of p24/ml) were injected at 0.2 μl/min by means of an automatic injector (Stoelting Co., Wood Dale, IL, USA). The animals received 2.4 μl of lentivirus at two sites, with the following coordinates: −4.8 rostral to bregma, 2.0 lateral to midline and −7.7 ventral from the skull surface, with the mouth bar set at −3.3 (site 1); −5.5 rostral to bregma, 1.7 lateral to midline, and −7.7 ventral from the skull surface, with the mouth bar set at −3.3 (site 2). LV expressing wild-type human ataxin-3 or mutant human ataxin-3 ($n = 8$) were injected in the left or right cortex. The animals received a single 4 μl injection of 125 000 ng of p24/ml lentivirus in each side at the following coordinates: −2.7 rostral to bregma, ±4 lateral to midline, and 4 ventral from the skull surface, with the mouth bar set at 0 (site 1). LV expressing wild-type human ataxin-3 or mutant human ataxin-3 ($n = 6$) were injected into the left and right striatum. The dose of vector particles administered was 125 000 or 250 000 ng of p24/ml for the dose/effect study ($n = 8$). The animals received a single 4 μl injection of lentivirus in each side at the following coordinates: 0.5 rostral to bregma, ±3 lateral to midline and 5 ventral from the skull surface, with the mouth bar set at 0 (site 1). After injection, the syringe needle was left in place for an additional 5 min before being slowly raised. The skin was closed using a 6–0 Prolene® suture (Ethicon, Johnson and Johnson, Brussels, Belgium).

Immunohistochemical procedure

Two months after lentiviral injection into the substantia nigra, 2 weeks and 2 months after injection in the striatum or 3 months after injection into the cortex, the animals were given a sodium pentobarbital overdose and were transcardially perfused with a phosphate solution followed by fixation with 4% PAF (Fluka, Sigma, Buchs, Switzerland) and 10% picric acid. The brains were removed and post-fixed in 4% PAF and 10% picric acid for 24 h and cryoprotected by incubation in 25% sucrose/0.1 M phosphate buffer for 48 h. The brains were frozen and 25 μm coronal sections were cut using a sliding microtome (Cryocut 1800, Leica Microsystems AG, Glattbrugg, Switzerland) at −20°C. Slices throughout the entire substantia nigra, cortex or striatum were collected in anatomical series and stored in 96-well trays (TPP, Switzerland) as free-floating sections in PBS supplemented with 0.12 μM sodium azide. The trays were stored at 4°C until immunohistochemical processing. Sections from injected rats were processed with the following primary antibodies: a mouse monoclonal anti-ataxin-3 antibody (1H9; 1:500; Chemicon, Temecula, CA, USA), recognizing the human ataxin-3 fragment from amino acids F112-L249 an affinity-purified rabbit polyclonal anti-TH antibody (AB152, 1:1000; Chemicon, Temecula, CA, USA); an affinity-purified rabbit polyclonal anti-vesicular monoamine transporter 2 (VMAT2) antibody (AB1767; 1:1000; Chemicon, Temecula, CA, USA); a rabbit polyclonal anti-ubiquitin antibody (Dako, 1:1000; Cambridgeshire, UK); a rabbit polyclonal anti-DARPP-32 antibody recognizing the 32 kDa dopamine- and cAMP-regulated phosphoprotein (AB1656; 1:5000); a mouse monoclonal anti-neuronal nuclei (NeuN) antibody (MAB377; 1:500; Chemicon, Temecula, CA, USA), followed by incubation with the respective biotinylated secondary antibodies (1:200; Vector Laboratories). Bound antibodies were visualized using the Vectastain ABC kit, with 3,3′-diaminobenzidine tetrahydrochloride (DAB metal concentrate; Pierce) as substrate. Degenerating neurons were stained with

the anionic fluorescein derivative Fluoro-Jade B (55). The sections were first washed in water and then mounted on sylanized glass slides, dehydrated and stained according to the supplier's manual (56).

Double stainings were performed for Ataxin-3 (1H9 Ab) and ubiquitin, for Ataxin-3 (1H9 Ab) and TH, for Ataxin-3 (1H9 Ab) and VMAT2 or Ataxin-3 (1H9 Ab) and α-synuclein (abcam ab6162). Free-floating sections from injected rats were processed with the described primary antibodies at RT for 1 h in PBS/0.1% Triton X-100 containing 10% NGS (Gibco) or 5% NDS (Normal Donkey Serum, Sigma, Saint Louis, MO, USA) (for Ataxin-3 and α-synuclein), then overnight at 4°C in blocking solution with the following antibodies: 1H9 (1:5000) and anti-ubiquitin (1:1000); 1H9 (1:5000) and anti-TH (1:1000), 1H9 (1:5000) and anti-VMAT2 (1:1000), 1H9 (1:5000) and anti-DARPP-32 (1:2000), polyclonal anti-ataxin-3 (1:2000), kindly provided by Dr Henry L. Paulson, anti-NeuN (1:500) or 1H9 (1:5000) and anti-α-synuclein (1:500) antibodies diluted in the respective blocking solution. Sections were washed three times and incubated for 2 h at RT with the corresponding secondary antibodies coupled to fluorophores (1:200; Molecular Probes, OR, USA) diluted in the respective blocking solution. The nuclear localization of ataxin-3 was investigated on sections double-stained for ataxin-3 (1H9 Ab) and Hoechst. The sections were washed three times and then mounted in Fluorsave Reagent (Calbiochem, Germany) on microscope slides.

Cresyl violet staining

Coronal 25 μm-thick striatal sections were cut using a freezing microtome (Cryocut 1800, Leica Microsystems AG, Glattbrugg, Switzerland). Premounted sections were stained with cresyl violet for 2 min, differentiated in acetate buffer pH 3.8–4 (2.72% sodium acetate and 1.2% acetic acid; 1:4 v/v), dehydrated by passing twice through ethanol and toluol solutions, and mounted onto microscope slides with Eukitt ® (O. Kindler GmbH & CO. Freiburg, Germany).

Transgenic mice

Mice (10–13 weeks old) were wild-type ($n = 4$) or Q71C homozygous transgenic mice ($n = 4$) expressing human mutant (Q71) ataxin-3 mjd1 under the control of the mouse prion promoter. Q71C homozygotes were at a late stage of the disease (25). Brains were cut using a freezing microtome (Cryocut 1800, Leica Microsystems AG, Glattbrugg, Switzerland) and immunohistochemistry was performed as described above, using anti-Ataxin-3 (1H9) (1:2000), anti-ubiquitin (1:1000) and anti-DARPP32 (1:4000) antibodies.

Human tissue

Postmortem striatal tissue from three MJD patients with morphologically and genetically confirmed MJD (61 ± 6 years, 71 ± 3 CAG number of mutant allele) and a 65-year-old control with no evidence of neurologic disease were obtained from the Neurology and Pathology Services, VA Medical Center, Albany Medical College, Albany, New York, NY, USA. The tissue was fresh when dissected and then placed in cold (4°C) at 10% neutral buffered formalin. Anti-ataxin-3 (1:1000) and anti-ubiquitin (1:1000) immunostainings were performed as previously described including the citrate buffer epitope retrieval method. Double stainings for Ataxin-3 (1H9; 1:2000; Chemicon, Temecula, CA, USA) and synuclein (anti-α-synuclein; No. 2628; 1:500; Cell Signaling), for ubiquitin (Dako, Cambridgeshire, 1:1000; UK) and synuclein (anti-α-β-synuclein; No. 2644; 1:500; Cell Signaling) were performed as previously described.

Behavioral analysis

Apomorphine-induced rotational asymmetry was measured three times before virus injection. Animals were injected subcutaneously with 1.0 mg/kg apomorphine (Amino AG, Neunhof, Switzerland) and placed into a test chamber (Rotoscan, Rotometer v5.06, Omnitech Instruments, Columbus, OH, USA) for a 3 min habituation period before a 45 min test session. Rotations were defined as complete 360° ipsilateral turns; the net difference between the two directions is reported. Animals that did not display spontaneous turning behavior (less than 20 turns per 45 min) were selected. Results are expressed as the net difference between the total number of turns before and after lesion. Ipsilateral turns were counted as positive turns, whereas contralateral turns were counted as negative turns.

Quantification of tyrosine hydroxylase-positive neurons

We used an Olympus CKX41 light microscope with a 10× magnification lens with a hand tally clicker counter to count TH-positive neurons in TH-stained coronal sections (200 μm between 25 μm thickness sections).

Evaluation of the volume of DARPP-32 depleted region

The extent of ataxin-3 lesions in the striatum was analyzed by digitizing ten DARPP-32-stained sections per animal (200 μm between 25 μm thickness sections), selected to obtain a complete rostrocaudal sampling of the striatum with a slide scanner and by quantifying the area of the lesion with a semi-automated image-analysis program (ImageJ software, NIH, MD, USA). Sections throughout the entire striatum were analyzed. The area of the striatum showing a loss of DARPP-32 staining was measured for each animal with an operator-independent macro. The volume was then estimated using the following formula: volume $= d(a1+a2+a3+\cdots)$, where d is the distance between serial sections (200 or 300 μm), and $a1$, $a2$, $a3$ etc. are DARPP-32-depleted areas for individual serial sections (57). The average gray value of all pixels measured in the lesioned area was recorded for each depleted area. Results are presented as the calculated value for volume of the DARPP-32 depleted region for each animal.

Statistical analysis

All quantifications are expressed as mean ± SEM. TH and DARPP-32 immunostaining statistical analyses were performed using one-way analysis of variance (ANOVA) followed by a Scheffe's protected least significant difference

post hoc test (StatView 4.0, version 3.2.6; Aladdin Systems). Statistical significance for rotational behavior was evaluated using the Friedman test, a non-parametric test for paired samples. Optical densities for DARPP-32 in wild-type and Q71C homozygous transgenic mice were analyzed using the Student's *t*-test. Significance thresholds were set at $P < 0.05$ for all tests.

SUPPLEMENTARY MATERIAL

Supplementary Material is available at HMG Online.

ACKNOWLEDGEMENTS

We thank Fabienne Pidoux, Maria de Fatima Rey, Christel Sadeghi, Anne Maillard, Philippe Colin, Gwennaelle Auregan, Jean-Yves Thuret, Régis Courbeyrette and Luísa Cortes for expert technical assistance, Pedro Anastácio for advice in statistical analysis and Dr. Henry L. Paulson for providing the polyclonal anti-ataxin-3 antibody.

Conflict of Interest statement. The authors declare no conflict of interest.

FUNDING

This work was funded by the Portuguese Foundation for Science and Technology (FCT—POCI/SAU-MMO/56055/2004, PTDC/SAU-FCF/70384/2006; L.P.A.); the National Ataxia Foundation (Grant No. 8 04/05; USA; L.P.A.); the Hereditary Disease Foundation (N.D.); Commissariat à l'Energie Atomique (CEA, N.D.).

REFERENCES

1. Sudarsky, L. and Coutinho, P. (1995) Machado-Joseph disease. *Clin. Neurosci. (NY)*, **3**, 17–22.
2. Kawaguchi, Y., Okamoto, T., Taniwaki, M., Aizawa, M., Inoue, M., Katayama, S., Kawakami, H., Nakamura, S., Nishimura, M., Akiguchi, I. *et al.* (1994) CAG expansions in a novel gene for Machado-Joseph disease at chromosome 14q32.1. *Nat. Genet.*, **8**, 221–228.
3. Doss-Pepe, E.W., Stenroos, E.S., Johnson, W.G. and Madura, K. (2003) Ataxin-3 interactions with rad23 and valosin-containing protein and its associations with ubiquitin chains and the proteasome are consistent with a role in ubiquitin-mediated proteolysis. *Mol. Cell. Biol.*, **23**, 6469–6483.
4. Chai, Y., Berke, S.S., Cohen, R.E. and Paulson, H.L. (2004) Poly-ubiquitin binding by the polyglutamine disease protein ataxin-3 links its normal function to protein surveillance pathways. *J. Biol. Chem.*, **279**, 3605–3611.
5. Burnett, B., Li, F. and Pittman, R.N. (2003) The polyglutamine neurodegenerative protein ataxin-3 binds polyubiquitylated proteins and has ubiquitin protease activity. *Hum. Mol. Genet.*, **12**, 3195–3205.
6. Donaldson, K.M., Li, W., Ching, K.A., Batalov, S., Tsai, C.C. and Joazeiro, C.A. (2003) Ubiquitin-mediated sequestration of normal cellular proteins into polyglutamine aggregates. *Proc. Nat. Acad. Sci. USA*, **100**, 8892–8897.
7. Scheel, H., Tomiuk, S. and Hofmann, K. (2003) Elucidation of ataxin-3 and ataxin-7 function by integrative bioinformatics. *Hum. Mol. Genet.*, **12**, 2845–2852.
8. Durr, A., Stevanin, G., Cancel, G., Duyckaerts, C., Abbas, N., Didierjean, O., Chneiweiss, H., Benomar, A., Lyon-Caen, O., Julien, J. *et al.* (1996) Spinocerebellar ataxia 3 and Machado-Joseph disease: clinical, molecular, and neuropathological features. *Ann. Neurol.*, **39**, 490–499.
9. Cummings, C.J. and Zoghbi, H.Y. (2000) Fourteen and counting: unraveling trinucleotide repeat diseases. *Hum. Mol. Genet.*, **9**, 909–916.
10. Cummings, C.J. and Zoghbi, H.Y. (2000) Trinucleotide repeats: mechanisms and pathophysiology. *Ann. Rev. Genomics Hum. Genet.*, **1**, 281–328.
11. Maciel, P., Costa, M.C., Ferro, A., Rousseau, M., Santos, C.S., Gaspar, C., Barros, J., Rouleau, G.A., Coutinho, P. and Sequeiros, J. (2001) Improvement in the molecular diagnosis of Machado-Joseph disease. *Arch. Neurol.*, **58**, 1821–1827.
12. Maruyama, H., Nakamura, S., Matsuyama, Z., Sakai, T., Doyu, M., Sobue, G., Seto, M., Tsujihata, M., Oh-i, T., Nishio, T. *et al.* (1995) Molecular features of the CAG repeats and clinical manifestation of Machado-Joseph disease. *Hum. Mol. Genet.*, **4**, 807–812.
13. Taroni, F. and DiDonato, S. (2004) Pathways to motor incoordination: the inherited ataxias. *Nat. Rev.*, **5**, 641–655.
14. Gwinn-Hardy, K., Singleton, A., O'Suilleabhain, P., Boss, M., Nicholl, D., Adam, A., Hussey, J., Critchley, P., Hardy, J. and Farrer, M. (2001) Spinocerebellar ataxia type 3 phenotypically resembling Parkinson disease in a black family. *Arch. Neurol.*, **58**, 296–299.
15. Fujigasaki, H., Uchihara, T., Koyano, S., Iwabuchi, K., Yagishita, S., Makifuchi, T., Nakamura, A., Ishida, K., Toru, S., Hirai, S. *et al.* (2000) Ataxin-3 is translocated into the nucleus for the formation of intranuclear inclusions in normal and Machado-Joseph disease brains. *Exp. Neurol.*, **165**, 248–256.
16. Fujigasaki, H., Uchihara, T., Takahashi, J., Matsushita, H., Nakamura, A., Koyano, S., Iwabuchi, K., Hirai, S. and Mizusawa, H. (2001) Preferential recruitment of ataxin-3 independent of expanded polyglutamine: an immunohistochemical study on Marinesco bodies. *J. Neurol. Neurosurg. Psychiatry*, **71**, 518–520.
17. Kettner, M., Willwohl, D., Hubbard, G.B., Rub, U., Dick, E.J., Jr, Cox, A.B., Trottier, Y., Auburger, G., Braak, H. and Schultz, C. (2002) Intranuclear aggregation of nonexpanded ataxin-3 in marinesco bodies of the nonhuman primate substantia nigra. *Exp. Neurol.*, **176**, 117–121.
18. Taniwaki, T., Sakai, T., Kobayashi, T., Kuwabara, Y., Otsuka, M., Ichiya, Y., Masuda, K. and Goto, I. (1997) Positron emission tomography (PET) in Machado-Joseph disease. *J. Neurol. Sci.*, **145**, 63–67.
19. Wullner, U., Reimold, M., Abele, M., Burk, K., Minnerop, M., Dohmen, B.M., Machulla, H.J., Bares, R. and Klockgether, T. (2005) Dopamine transporter positron emission tomography in spinocerebellar ataxias type 1, 2, 3 and 6. *Arch. Neurol.*, **62**, 1280–1285.
20. Yen, T.C., Tzen, K.Y., Chen, M.C., Chou, Y.H., Chen, R.S., Chen, C.J., Wey, S.P., Ting, G. and Lu, C.S. (2002) Dopamine transporter concentration is reduced in asymptomatic Machado-Joseph disease gene carriers. *J. Nucl. Med.*, **43**, 153–159.
21. Lee, W.Y., Jin, D.K., Oh, M.R., Lee, J.E., Song, S.M., Lee, E.A., Kim, G.M., Chung, J.S. and Lee, K.H. (2003) Frequency analysis and clinical characterization of spinocerebellar ataxia types 1, 2, 3, 6 and 7 in Korean patients. *Arch. Neurol.*, **60**, 858–863.
22. Ishikawa, A., Yamada, M., Makino, K., Aida, I., Idezuka, J., Ikeuchi, T., Soma, Y., Takahashi, H. and Tsuji, S. (2002) Dementia and delirium in 4 patients with Machado-Joseph disease. *Arch. Neurol.*, **59**, 1804–1808.
23. Ikeda, H., Yamaguchi, M., Sugai, S., Aze, Y., Narumiya, S. and Kakizuka, A. (1996) Expanded polyglutamine in the Machado-Joseph disease protein induces cell death in vitro and in vivo. *Nat. Genet.*, **13**, 196–202.
24. Cemal, C.K., Carroll, C.J., Lawrence, L., Lowrie, M.B., Ruddle, P., Al-Mahdawi, S., King, R.H., Pook, M.A., Huxley, C. and Chamberlain, S. (2002) YAC transgenic mice carrying pathological alleles of the MJD1 locus exhibit a mild and slowly progressive cerebellar deficit. *Hum. Mol. Genet.*, **11**, 1075–1094.
25. Goti, D., Katzen, S.M., Mez, J., Kurtis, N., Kiluk, J., Ben-Haiem, L., Jenkins, N.A., Copeland, N.G., Kakizuka, A., Sharp, A.H. *et al.* (2004) A mutant ataxin-3 putative-cleavage fragment in brains of Machado-Joseph disease patients and transgenic mice is cytotoxic above a critical concentration. *J. Neurosci.*, **24**, 10266–10279.
26. Bichelmeier, U., Schmidt, T., Hubener, J., Boy, J., Ruttiger, L., Habig, K., Poths, S., Bonin, M., Knipper, M., Schmidt, W.J. *et al.* (2007) Nuclear localization of ataxin-3 is required for the manifestation of symptoms in SCA3: in vivo evidence. *J. Neurosci.*, **27**, 7418–7428.
27. de Almeida, L.P., Ross, C.A., Zala, D., Aebischer, P. and Deglon, N. (2002) Lentiviral-mediated delivery of mutant huntingtin in the striatum of rats induces a selective neuropathology modulated by polyglutamine repeat size, huntingtin expression levels, and protein length. *J. Neurosci.*, **22**, 3473–3483.

28. Lo Bianco, C., Ridet, J.L., Schneider, B.L., Deglon, N. and Aebischer, P. (2002) Alpha-synucleinopathy and selective dopaminergic neuron loss in a rat lentiviral-based model of Parkinson's disease. *Proc. Nat. Acad. Sci. USA*, **99**, 10813–10818.
29. Kirik, D., Annett, L.E., Burger, C., Muzyczka, N., Mandel, R.J. and Bjorklund, A. (2003) Nigrostriatal alpha-synucleinopathy induced by viral vector-mediated overexpression of human alpha-synuclein: a new primate model of Parkinson's disease. *Proc. Nat. Acad. Sci. USA*, **100**, 2884–2889.
30. Lauwers, E., Debyser, Z., Van Dorpe, J., De Strooper, B., Nuttin, B. and Baekelandt, V. (2003) Neuropathology and neurodegeneration in rodent brain induced by lentiviral vector-mediated overexpression of alpha-synuclein. *Brain Pathol.*, **13**, 364–372.
31. de Almeida, L.P., Zala, D., Aebischer, P. and Deglon, N. (2001) Neuroprotective effect of a CNTF-expressing lentiviral vector in the quinolinic acid rat model of Huntington's disease. *Neurobiol. Dis.*, **8**, 433–446.
32. Paulson, H.L., Bonini, N.M. and Roth, K.A. (2000) Polyglutamine disease and neuronal cell death. *Proc. Nat. Acad. Sci. USA*, **97**, 12957–12958.
33. Lokkegaard, T., Nielsen, J.E., Hasholt, L., Fenger, K., Werdelin, L., Tranebjaerg, L., Lauritzen, M., Colding-Jorgensen, E., Gronbech-Jensen, M., Henriksen, O.A. *et al.* (1998) Machado-Joseph disease in three Scandinavian families. *J. Neurol. Sci*, **156**, 152–157.
34. Soong, B., Cheng, C., Liu, R. and Shan, D. (1997) Machado-Joseph disease: clinical, molecular, and metabolic characterization in Chinese kindreds. *Ann. Neurol.*, **41**, 446–452.
35. Tait, D., Riccio, M., Sittler, A., Scherzinger, E., Santi, S., Ognibene, A., Maraldi, N.M., Lehrach, H. and Wanker, E.E. (1998) Ataxin-3 is transported into the nucleus and associates with the nuclear matrix. *Hum. Mol. Genet.*, **7**, 991–997.
36. Trottier, Y., Cancel, G., An-Gourfinkel, I., Lutz, Y., Weber, C., Brice, A., Hirsch, E. and Mandel, J.L. (1998) Heterogeneous intracellular localization and expression of ataxin-3. *Neurobiol. Dis.*, **5**, 335–347.
37. Carvalho, A.L., Cortes, L., Maciel, P. and Macedo-Ribeiro, S. (2005) *Neuroscience S.f. Abstract Viewer/Itinerary Planner [Online]*. Washington, DC, Program No. 427.8. 2005.
38. Perez, M.K., Paulson, H.L., Pendse, S.J., Saionz, S.J., Bonini, N.M. and Pittman, R.N. (1998) Recruitment and the role of nuclear localization in polyglutamine-mediated aggregation. *J. Cell Biol.*, **143**, 1457–1470.
39. Perez, M.K., Paulson, H.L. and Pittman, R.N. (1999) Ataxin-3 with an altered conformation that exposes the polyglutamine domain is associated with the nuclear matrix. *Hum. Mol. Genet.*, **8**, 2377–2385.
40. Paulson, H.L., Perez, M.K., Trottier, Y., Trojanowski, J.Q., Subramony, S.H., Das, S.S., Vig, P., Mandel, J.L., Fischbeck, K.H. and Pittman, R.N. (1997) Intranuclear inclusions of expanded polyglutamine protein in spinocerebellar ataxia type 3. *Neuron*, **19**, 333–344.
41. Chen, S., Berthelier, V., Hamilton, J.B., O'Nuallain, B. and Wetzel, R. (2002) Amyloid-like features of polyglutamine aggregates and their assembly kinetics. *Biochemistry*, **41**, 7391–7399.
42. Bevivino, A.E. and Loll, P.J. (2001) An expanded glutamine repeat destabilizes native ataxin-3 structure and mediates formation of parallel beta -fibrils. *Proc. Nat. Acad. Sci. USA*, **98**, 11955–11960.
43. Poirier, M.A., Li, H., Macosko, J., Cai, S., Amzel, M. and Ross, C.A. (2002) Huntingtin spheroids and protofibrils as precursors in polyglutamine fibrilization. *J. Biol. Chem.*, **277**, 41032–41037.
44. Tanaka, M., Machida, Y., Nishikawa, Y., Akagi, T., Hashikawa, T., Fujisawa, T. and Nukina, N. (2003) Expansion of polyglutamine induces the formation of quasi-aggregate in the early stage of protein fibrillization. *J. Biol. Chem.*, **278**, 34717–34724.
45. Gales, L., Cortes, L., Almeida, C., Melo, C.V., do Carmo Costa, M., Maciel, P., Clarke, D.T., Damas, A.M. and Macedo-Ribeiro, S. (2005) Towards a structural understanding of the fibrillization pathway in Machado-Joseph's disease: trapping early oligomers of non-expanded ataxin-3. *J. Mol. Biol.*, **353**, 642–654.
46. Macedo-Ribeiro, S., Pereira de Almeida, L., Carvalho, A. and Rego, A. (2007) Malva, J., Rego, A., Oliveira, C. and Cunha, R. (eds), *Interactions Between Neurons and Glia in Aging and Disease*, Springer.
47. Boeddrich, A., Gaumer, S., Haacke, A., Tzvetkov, N., Albrecht, M., Evert, B.O., Muller, E.C., Lurz, R., Breuer, P., Schugardt, N. *et al.* (2006) An arginine/lysine-rich motif is crucial for VCP/p97-mediated modulation of ataxin-3 fibrillogenesis. *EMBO J.*, **25**, 1547–1558.
48. Mao, Y., Senic-Matuglia, F., Di Fiore, P.P., Polo, S., Hodsdon, M.E. and De Camilli, P. (2005) Deubiquitinating function of ataxin-3: insights from the solution structure of the Josephin domain. *Proc. Nat. Acad. Sci. USA*, **102**, 12700–12705.
49. Matsumoto, M., Yada, M., Hatakeyama, S., Ishimoto, H., Tanimura, T., Tsuji, S., Kakizuka, A., Kitagawa, M. and Nakayama, K.I. (2004) Molecular clearance of ataxin-3 is regulated by a mammalian E4. *EMBO J.*, **23**, 659–669.
50. Berke, S.J., Chai, Y., Marrs, G.L., Wen, H. and Paulson, H.L. (2005) Defining the role of ubiquitin-interacting motifs in the polyglutamine disease protein, ataxin-3. *J. Biol. Chem.*, **280**, 32026–32034.
51. Warrick, J.M., Morabito, L.M., Bilen, J., Gordesky-Gold, B., Faust, L.Z., Paulson, H.L. and Bonini, N.M. (2005) Ataxin-3 suppresses polyglutamine neurodegeneration in Drosophila by a ubiquitin-associated mechanism. *Mol. Cell*, **18**, 37–48.
52. Klockgether, T., Skalej, M., Wedekind, D., Luft, A.R., Welte, D., Schulz, J.B., Abele, M., Burk, K., Laccone, F., Brice, A. *et al.* (1998) Autosomal dominant cerebellar ataxia type I. MRI-based volumetry of posterior fossa structures and basal ganglia in spinocerebellar ataxia types 1, 2 and 3. *Brain*, **121** (Pt. 9), 1687–1693.
53. Janavs, J.L. and Aminoff, M.J. (1998) Dystonia and chorea in acquired systemic disorders. *J. Neurol. Neurosurg. Psychiatry*, **65**, 436–445.
54. Hottinger, A.F., Azzouz, M., Deglon, N., Aebischer, P. and Zurn, A.D. (2000) Complete and long-term rescue of lesioned adult motoneurons by lentiviral-mediated expression of glial cell line-derived neurotrophic factor in the facial nucleus. *J. Neurosci.*, **20**, 5587–5593.
55. Schmued, L.C. and Hopkins, K.J. (2000) Fluoro-Jade B: a high affinity fluorescent marker for the localization of neuronal degeneration. *Brain Res.*, **874**, 123–130.
56. Schmued, L.C., Albertson, C. and Slikker, W., Jr (1997) Fluoro-Jade: a novel fluorochrome for the sensitive and reliable histochemical localization of neuronal degeneration. *Brain Res.*, **751**, 37–46.
57. Reynolds, D.S., Carter, R.J. and Morton, A.J. (1998) Dopamine modulates the susceptibility of striatal neurons to 3-nitropropionic acid in the rat model of Huntington's disease. *J. Neurosci.*, **18**, 10116–10127.